Determination of Λdoublet resolved crosssections for inelastic scattering of OH by para and normalH2

K. Schreel and J.J. ter Meulen

Citation: The Journal of Chemical Physics **105**, 4522 (1996); doi: 10.1063/1.472328
View online: http://dx.doi.org/10.1063/1.472328
View Table of Contents: http://scitation.aip.org/content/aip/journal/jcp/105/11?ver=pdfcov
Published by the AIP Publishing

Determination of Λ-doublet resolved cross-sections for inelastic scattering of OH by para- and normal-H_2

K. Schreel and J.J. ter Meulen
Molecular and Laser Physics, University of Nijmegen, P.O Box 9010, 6500 GL Nijmegen, The Netherlands

(Received 18 March 1996; accepted 10 June 1996)

In this paper we report the measurement of Λ-doublet resolved state-to-state cross sections for inelastic collisions of OH by H_2 at a translational energy of 595 cm^{-1}. Experimental values are obtained for transitions from both the upper (f) and the lower (e) Λ-doublet substates of the lowest rotational state $(J = \frac{3}{2})$ of OH($^2\Pi_{3/2}$) to almost all other states within the range of the collision energy. Cross sections for scattering by both para- and normal-H_2 have been determined. The main difference between para- and normal-H_2 scattering is seen in the Λ-doublet cross section. The results are compared to He-scattering which shows that H_2 $(J = 0)$ scattering behaves similar to He scattering. When averaged over the Λ-doublet states, the cross sections are in good agreement with the measurements of Andresen *et al.* [J. Chem. Phys. **81**, 571 (1984)], although the conclusions with regard to collisional pumping of interstellar OH masers are different. The quantum calculations of Offer *et al.* [J. Chem. Phys. **100**, 362 (1994)] show a surprisingly good correspondence with the measured values. In this comparison the full initial state distribution of the OH and H_2 beams has been taken into account. © *1996 American Institute of Physics.* [S0021-9606(96)00235-8]

I. INTRODUCTION

The OH-H_2 system has been attracting a lot of interest in the past years. There are several reasons for this. First of all the rotational energy transfer of OH in collisions with H_2 is believed to be a dominant process governing the population distribution of the hydroxyl radicals in the interstellar space and thereby the conditions which give rise to the observed maser action.[1–4] Second, the reaction $OH + H_2 \rightleftharpoons H_2O + H$ is a prototypical reaction in reaction dynamics, on which a number of experimental and theoretical studies has been published in the past years.[5–8] Third, the van der Waals complex OH–H_2, which recently has been observed by Loomis and Lester,[9] is the first known van der Waals bound complex of two mutually reactive species. Calculations on the spectrum of this complex have been made by Clary and co-workers.[10–12]

In 1973 Gwinn *et al.*[13] were the first to describe a model based on collisional pumping of interstellar OH molecules and subsequent ir radiative decay, producing population inversion of the lowest Λ-doublet states. This paper, as well as later publications[14] on interstellar OH pumping by H_2, was, however, based on an incorrectly assigned symmetry to the Λ-doublet states.[15,16] In more recent collisional models, maser emission is predicted in either the $\Pi_{3/2}$, or the $\Pi_{1/2}$ multiplet state, or in both, depending on the local infrared radiation intensities and H_2 densities.[17–19] In these models the cross sections for excitation of OH by H_2 are approximated by taking calculated values for either OH–para-$H_2(J=0)$ collisions, or OH–He collisions, corrected for the mass difference between He and H_2. The need for reliable state-to-state cross sections is strongly emphasized by all authors.

Despite this strong interest in the OH–H_2 system only one experimental study to the rotational excitation of OH by H_2 has been reported.[20,21] In this experiment Andresen and coworkers obtained cross sections for collision induced transitions from the rotational ground state $^2\Pi_{3/2}, J=\frac{3}{2}$. Since both Λ-doublet states of this state were (equally) populated, the obtained results are averaged cross sections for transitions from the upper (f) and lower (e) doublet states. The authors observed a clear preference for selective excitation of lower Λ-doublet states in the $\Pi_{3/2}$ rotational ladder and of upper Λ-doublet states in the $\Pi_{1/2}$ rotational ladder. This observation has given rise to a number of theoretical studies in which the results of close coupling calculations were compared to the experimental values.[16,21–24] The calculations were all based on the *ab-initio* potential of Kochanski and Flower,[25] and involved only para-H_2 in $J=0$. In the experiment of Andresen *et al.* however, normal-H_2 was used at about 300 K, containing a fraction of $H_2(J=0)$ smaller than 15%. Recently Miller *et al.* reported calculations on rotationally inelastic collisions of OH by both ortho- and para-H_2 using an *ab-initio* potential based on the coupled electron pair approximation (CEPA).[10] The authors considered only planar geometries for the OH–H_2 system, and consequently described their results in relation to a sum and a difference potential, $V_{A'}+V_{A''}$ and $V_{A'}-V_{A''}$, respectively (according to the irreducible representation of the C_s point group). Deviations between the calculated cross sections for multiplet changing transitions and the experimental results of Andresen *et al.* were ascribed to defects in the difference potential. In the same paper Miller *et al.* report calculated values for the energies of the van der Waals bound states and rovibrational transition frequencies. The only potential including non-planar geometries of OH–H_2 has been published by Offer and Van Hemert.[26] According to the authors this potential should give an improved description of the dependence of the potential on the orientation of the H_2 molecule. Based on this potential, theoretical calculations for para-$H_2(J=0,2)$ and ortho-$H_2(J=1)$ have been published.[27]

Where spectroscopy of the van der Waals complex pro-

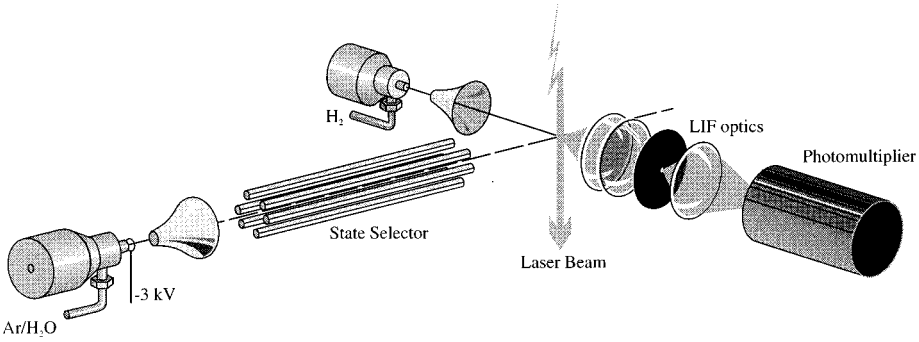

FIG. 1. A schematical drawing of the experimental setup. The relative sizes of the objects are not to scale.

vides detailed information about the attractive well of the potential energy surface, the determination of state-to-state cross sections provides direct information about both the attractive and the repulsive part of the potential. Most relevant is the comparison between OH–para-H_2 and OH–ortho-H_2 dynamics, particularly because in the interstellar space the ratio of ortho- and para-H_2 may be different from the equilibrium value 3, which might even be used as an indication of the age of clouds.[28] Furthermore, one expects $H_2(J=0)$ to behave differently from $H_2(J\geqslant 1)$ because for $J=0$ the quadrupole term in the interaction potential does not give a contribution to the inelastic collision process.[29] In that case H_2 should behave very similar to He.

We have determined the Λ-doublet resolved cross sections of the OH–H_2 system in a crossed molecular beam experiment. State selection of the OH molecules by an electrostatic hexapole resulted in an almost true state-to-state experiment. By combining measurements with and without state selector, we were able to determine the cross sections for transitions from both Λ-doublet states of the lowest rotational state. No single state H_2 beam could be produced, but by comparing cross sections obtained with beams of different temperatures we were able to estimate the effect of the higher rotational states.

II. EXPERIMENT

A. Setup

The experimental setup as shown in Fig. 1 is almost the same as in previous experiments,[30,31] but will be outlined briefly below.

The crossed molecular beam setup is formed by two vacuum chambers. The larger chamber is used for both the OH beam source and the collision area. A movable plate divides this chamber in two. In this plate a skimmer is mounted to form the OH beam. Each half of the chamber is pumped by a diffusion pump. The other chamber is used for the H_2 source and is placed perpendicular to the OH beam axis. The pulsed valve as well as the skimmer plate of the OH beam are mounted on two rods in a way that they can be moved forwards and backwards with respect to the collision center. An electrostatic hexapole can also be mounted on the rods, between the shielding plate and the collision area.

The beam sources are two modified Bosch-type pulsed valves with a pulse width of approximately 1 ms. The valves have a nozzle diameter of 1 mm. The H_2 valve can be equipped with a nozzle cap having an opening of 0.3 mm. Both normal-H_2 (a 3:1 mixture of ortho- and para-H_2) and para-H_2 are used as collision partner for the OH molecules. The OH beam is produced by expanding an H_2O (18 Torr, vapor pressure at room temperature) in argon (1.5 bar) mixture. A ring shaped electrode with an internal diameter of 4 mm, which is kept at a negative high voltage (-3 kV), is placed in front of the nozzle orifice at a distance of 1 mm. During the expansion an electrical discharge between the electrode and the valve dissociates the H_2O molecules while forming OH. Because of the rotational cooling during the expansion, the lowest rotational state ($^2\Pi_{3/2},J=\frac{3}{2}$)is predominantly occupied: 90% of the OH molecules are in this Λ-doublet split state. The first excited rotational state ($^2\Pi_{3/2},J=\frac{5}{2}$)lying at 84 cm^- above the ground rotational state, as shown in Fig. 2, is occupied by 8% of the total amount of OH molecules.

Two different types of experiments were performed. One in which an electrostatic hexapole was inserted in the OH beam behind the skimmer and one without the hexapole. The hexapole focuses molecules in the upper $J=\frac{3}{2}$ Λ-doublet state (f) and defocuses molecules in the lower Λ-doublet state (e). By performing measurements with and without state selector it is possible to extract information about the collisional dynamics of OH molecules in both the upper and the lower Λ-doublet states. The hexapole has an inner radius of 3 mm and the length is 24 cm. A voltage difference of 20 kV between the rods results in the maximum beam intensity at the collision center, at a distance of 10 cm from the end of the hexapole.

Detection of the OH state distributions with and without collisions is performed by laser induced fluorescence (LIF) spectroscopy of the $A\leftarrow X$ electronic transition at 308 nm. Each line in the spectrum is uniquely assignable to a single rotational and Λ-doublet state in the ground electronic state.[32] The lines used to determine the cross sections for the collision induced transitions to the $\Pi_{3/2},J$ states are $Q_1(N)$ and $P_1(N)$ with $N=J-\frac{1}{2}$ ranging from 1 to 4. The cross sections for transitions to the $\Pi_{1/2},J$ states are measured by the $Q_2(N)$ and the $P_2(N)$ transitions with $N=J+\frac{1}{2}$

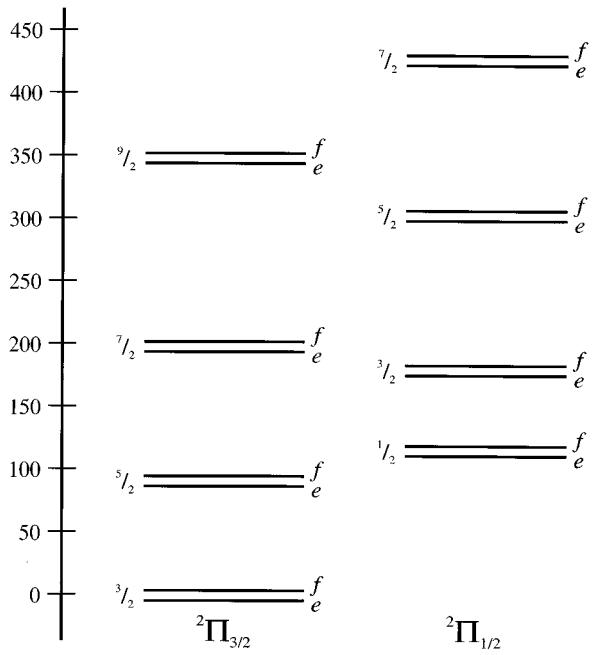

FIG. 2. An overview of the lowest rotational levels of OH ($X^2\Pi$). The splitting of the Λ-doublets is greatly exaggerated.

ranging from 1 to 3. The upper (f) Λ-doublet states are probed by the Q transitions, the lower (e) Λ-doublet states by the P transitions. The $Q_2(2)$ and $Q_2(3)$ lines are coincident within the bandwidth of the laser. The measured cross section at these transitions represents in fact the sum of the cross sections for transitions to the $^2\Pi_{1/2}, J=\frac{3}{2}$ and $J=\frac{5}{2}$ states.

The fluorescence at 308 nm is collected by lenses and imaged onto a photomultiplier. In front of the photomultiplier a UG-11 filter was installed to suppress stray light and all visible radiation originating from the discharge. The laser used in this experiment is a dye laser (Lambda Physik FL 2002) pumped by an excimer laser (Lambda Physik EMG 201 MSC). The power of the frequency doubled output of the dye laser operating with rhodamine B dye, is in the order of 1 mJ. This is enough to saturate all transitions in the LIF spectrum. The measured relative intensities are thus a direct measure for the relative population of the probed states.

Because of the nuclear spin $\frac{1}{2}$ of the H atom, the homonuclear H_2 molecule is present in two ''varieties:'' ortho ($I=1$, odd J-values) and para ($I=0$, even J-values). Due to nuclear spin statistics the ''natural'' ratio of the ortho versus the para variety is $3\div1$. This gas will be referred to as normal-H_2. Also use has been made of nearly pure para-H_2, which is produced using a converter.[33] In this setup normal-H_2 is flowed over a catalyst (iron-oxide) at temperatures near the liquefaction temperature of hydrogen (25 K). The H_2 molecules are absorbed on the surface of the catalyst where the spins of the two nuclei are decoupled due to the high local magnetic field. Upon desorption the spins are recoupled but now in the lowest rotational state which forces it to be para. The reconversion of para to normal has a rate of a few percent per week at room temperature and 1 atm if not in the presence of any ferromagnetic material.[33] The para-H_2 is produced on line while performing the collision experiment.

TABLE I. Initial relative populations (in %) of the OH beam. Relative populations below 1% have been neglected. The labels ''upper Λ-doublet'' and ''lower Λ-doublet'' refer to the states which are preferentially selected. The population of the lower Λ-doublet state is the effective remaining population after subtraction of the cross sections obtained with hexapole from the cross sections obtained without hexapole.

State			
J	ϵ	Upper Λ-doublet	Lower Λ-doublet
3/2	e		96.5
3/2	f	93.5	
5/2	e		3.5
5/2	f	6.5	

B. Initial state distribution

In an ideal state-to-state collision experiment the scattering process involves only one single collision, by which an energy transfer is induced between a prepared single initial state and a final state which can be probed. The initial and final state distribution should be known for both scattering partners. In this crossed beam experiment, the single collision condition regime is obtained by adjusting the beam intensity of secondary molecules to such a low value that the population transfer is linear with the density.[31] The initial state distribution, however, is not 100% pure and a full characterization of both the OH and the H_2 beams is required.

1. The OH beam

Initial state preparation of the OH radicals is achieved by rotational cooling in the supersonic expansion of the OH/Ar molecular pulse, and by state selection via the electrostatic hexapole. Characterization is performed by probing the initial population via the same LIF technique which is used for measuring the cross sections. This has been worked out in a previous paper.[30] The results are that after the expansion 90% of the OH molecules is in the lowest rotational state ($\Omega=\frac{3}{2}, J=\frac{3}{2}$). In the OH production and/or subsequent rotational cooling a Λ-doublet population inversion takes place which results in a higher population of the upper Λ-doublet level than the population of the lower level ($100\div68$). This might be due to the electrical discharge being the production method. This behavior is not observed when the OH is produced by photodissociation.

When the population of states containing less than 1% of the total population is neglected, then, after electrostatic state selection, 93.5% of the population is contained in the $\frac{3}{2},f$ state and 6.5% in the $\frac{5}{2},f$ state. After subtracting the measurements with state selector from the measurements without state selector and neglecting states with a population less than 1%, a population resulted of 96.5% in the $\frac{3}{2},e$ state and 3.5% in the $\frac{5}{2},e$ state. These results are summarized in Table I.

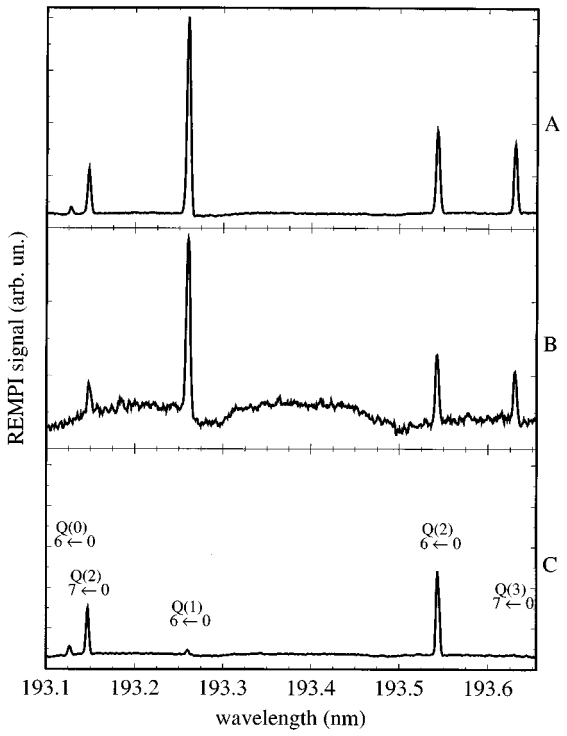

FIG. 3. Measured H_2 spectrum via 2+1 REMPI of the $E(v''=6,7)\leftarrow X(v'=0)$ transition. (A) measurement of normal-H_2, (B) measurement of thermalized H_2 (C) measurement of para-H_2. The curved baseline in (B) is caused by power variations of the excimer laser.

2. The H_2 beam

Characterization of the H_2 beam served two purposes: determination of the rotational population distribution and determination of the purity of the para-H_2 which is produced in the converter. Resonance enhanced multiphoton ionization spectroscopy (REMPI) was applied to determine the H_2 population distribution at the collision center. For this purpose a Wiley–McLaren[34] type time-of-flight tube was mounted in the collision center with the lower two plates centered around the H_2 beam with a spacing between the plates of 2.5 cm and a tube length of 10 cm. A mass resolution of 50 was obtained. In the tube a ring was mounted which acts as an electrostatic lens to correct for a divergence of the ions caused by the small dimensions of the plates.

Two experiments were performed. One in which the population distribution of the ''warm'' beam and the purity of the para-H_2 was determined and one in which the population distribution of the ''cold'' beam was measured. In these experiments two different lasers and detection schemes were used.

The first experiment involved the use of a tunable ArF excimer laser (Lambda Physik EMG 150 MSC), tunable from 193.1 to 193.8 nm. Two-photon excitation of part of the $E^1\Sigma_g^+(v''=6,7)\leftarrow X^1\Sigma_g^+(v'=0)$ band[35–37] and subsequent ionization by a third photon resulted in a spectrum as shown in Fig. 3(A). The position of the $J=0$ line is on the edge of the tuning curve of the laser which results in a relatively small signal. To determine the population in the beam this spectrum was compared to a spectrum of thermalized gas when the vacuum chamber was filled with 10^{-4} Torr H_2, as shown in Fig. 3(B). The curved baseline is caused by nonresonant ionization and is a reflection of the wavelength dependence of the power of the excimer laser. In Fig. 3(C) a spectrum is presented when a beam of para-H_2 is used. It can clearly be seen that the signal of transitions starting from odd J-values is strongly reduced. Note that this spectrum has been recorded after the molecules have passed through the (magnetic) pulsed valve. So any conversion which might have taken place in the valve has been accounted for. From these measurements the results are derived as presented in Table II.

TABLE II. Initial relative populations (in %) of the H_2 beam.

	Normal H_2		para H_2	
State	''warm''	''cold''	''warm''	''cold''
$J=0$	12.0	16.7	44.2	61.7
$J=1$	65.1	73.5	6.5	7.3
$J=2$	13.0	8.3	48.3	30.8
$J=3$	9.9	1.5	1.0	0.2

As can be seen from Table II, the higher rotational levels are relatively strongly populated in the ''warm'' beam. Especially in the para-H_2 case the presence of an equal amount of molecules in the $J=2$ and $J=0$ states might conceal the expected deviating behavior of $J=0$ molecules in inelastic collisions. We therefore investigated the possibilities of producing a colder H_2 beam. We found that mounting a cap in front of the valve with a much smaller nozzle diameter (0.3 mm versus 1.0 mm) resulted in a significantly colder beam. Unfortunately a strong cooling of the valve itself (e.g., by liquid nitrogen) turned out to be technically impossible.

The population distribution of this ''cold'' H_2 beam was measured using a different detection scheme as opposed to the ''warm'' H_2 measurements because the tunable excimer laser was not available at that time. Instead we used a Nd:YAG (Continuum YG-681-C10) pumped dye laser (Continuum TDL-60) operating on rhodamine B dye to excite the $C^1\Pi_u(v=1)\leftarrow X^1\Sigma_g^+(v=0)$ transition around 296 nm[38] via 3+1 REMPI. The maximum output of the frequency doubled radiation was 14 mJ. However, only 1.5 mJ was used in order to avoid non-linear effects. The radiation was focused by a 25 cm quartz lens into the vacuum chamber. The detection setup was exactly the same as in the case of the (2+1) REMPI experiment.

The same set of measurements was performed as for the ''warm'' H_2 beam, leading to the results as presented in Table II. As can be seen, the lowest rotational levels are much more populated than in the case of ''warm'' H_2, but, unfortunately, the beam is still far off from being rotationally cold. Nevertheless, the difference in population of the $J=2$ level of the ''warm'' and ''cold'' beam is large enough to estimate its influence on the measured cross sections.

C. Data reduction

Each state is probed by averaging the signal of 1000 laser shots both with and without collisions, while the laser frequency is fixed on top of the line. The power density of the laser radiation in the collision area is high enough to saturate all OH transitions. So the observed increase in LIF signal on the excited rotational states is directly proportional to the increase in population of these states, and hence directly proportional to the cross section of the collisional induced transition involved. The average of 4–6 measurements is used to determine the relative cross section, which is taken to be the increase in population of the excited state, divided by the decrease in population of the initial state. The sum of all cross sections always equaled one within the assigned error. This indicates that all scattered molecules are detected, regardless of their final velocity.

When use is made of the hexapole, the change in population of the collisionally excited states, denoted by ΔN_k, can be expressed as

$$\Delta N_k = N_f \sigma'_{f\to k}, \tag{1}$$

where N_f is the initial population of the $\frac{3}{2},f$ state, and $\sigma'_{f\to k}$ is the absolute cross section for the transition to the state labeled by k, multiplied by the (unknown) secondary beam density and interaction path length. The measured relative cross section is then given by

$$\sigma_{f\to k} = \frac{\Delta N_k}{\Delta N_f} = \frac{N_f \sigma'_{f\to k}}{\Delta N_f}, \tag{2}$$

where $-\Delta N_f$ is the collision induced decrease of the initial state population.

For the special case of the Λ-doublet transition, the measured cross section will be denoted as

$$\sigma_{f\to e} = \frac{N_f \sigma'_{f\to e}}{\Delta N_f} \equiv \sigma_\Lambda, \tag{3}$$

where the $\frac{3}{2},e$ state is labeled with e.

Also measurements without hexapole have been performed. In this case both the $\frac{3}{2},f$ and the $\frac{3}{2},e$ states are present in the beam. The purpose was to derive cross sections for transitions starting from the $\frac{3}{2},e$ state by subtracting the data obtained with hexapole from the data obtained without hexapole. This subtraction procedure is, however, not straightforward. In the case without hexapole, the increase in population of the excited rotational states is due to a contribution of both initial states. The decrease in population of each of the two initial states is a combination of outscattering towards all other states including the other Λ-doublet state, and *in*scattering from the other Λ-doublet state. Because the population of both initial states is not equal, scattering from one initial state to the other is not canceled by the reverse transition. This situation can be described as follows.

Let, for scattering without hexapole, $-\Delta n_e$ and $-\Delta n_f$ be the collision induced decreases of the population of the upper and lower $J = \frac{3}{2}$ Λ-doublet states, respectively. Here a lower case n is used to distinguish between the cases with and without hexapole. In the case of small population changes, when the single collision condition is fulfilled, the following relations hold:

$$-\Delta n_e = n_f \sigma'_{f\to e} - n_e \sigma'_{e\to f} - n_e \sum_k \sigma'_{e\to k}, \tag{4}$$

$$-\Delta n_f = n_e \sigma'_{e\to f} - n_f \sigma'_{f\to e} - n_f \sum_k \sigma'_{f\to k}, \tag{5}$$

where n_f and n_e are the initial population of the upper and lower states, respectively.

The quantities which are measured during the experiment are $\Delta n_f/n_f$, $\Delta n_e/\Delta n_f$ and the various $\Delta n_k/\Delta n_f$ in which k ranges over all states except the $\frac{3}{2},e$ and $\frac{3}{2},f$ states. The latter quantity is composed of two contributions

$$\frac{\Delta n_k}{\Delta n_f} = \frac{\Delta n_{f\to k} + \Delta n_{e\to k}}{\Delta n_f}. \tag{6}$$

Here $\Delta n_{f\to k}$ and $\Delta n_{e\to k}$ represent the increase in population of the state k caused by a transition from the $\frac{3}{2},f$ and $\frac{3}{2},e$ state, respectively. The quantities $\Delta N_k/\Delta N_f$ and $\Delta n_{f\to k}/\Delta n_f$ involve the same relative cross section $\sigma'_{f\to k}$, but they are different, since Δn_f involves also the cross sections for the Λ-doublet transitions, $\sigma'_{e\to f}$ and $\sigma'_{f\to e}$. It is however possible to determine one scaling factor for all k, which relates $\Delta N_k/\Delta N_f$ to $\Delta n_{f\to k}/\Delta n_f$. This scaling factor, denoted with S, is defined by

$$S\frac{\Delta N_k}{\Delta N_f} = \frac{\Delta n_{f\to k}}{\Delta n_f} \tag{7}$$

or, when summed over k

$$S\sum_k \frac{\Delta N_k}{\Delta N_f} = \sum_k \frac{\Delta n_{f\to k}}{\Delta n_f} \tag{8}$$

with k again ranging over all states except the two Λ-doublet states. Where the sum on the left hand side follows directly from the measured values, the sum on the right hand side is obtained indirectly from the experiment, as is shown below.

In the case without hexapole, the total outscattering from both initial states to all other states except the two initial states, denoted with $\Delta n'_f$ and $\Delta n'_e$, respectively, is given by

$$\Delta n'_f = \sum_k \Delta n_{f\to k} = n_f \sum_k \sigma'_{f\to k}, \tag{9}$$

$$\Delta n'_e = \sum_k \Delta n_{e\to k} = n_e \sum_k \sigma'_{e\to k}. \tag{10}$$

Similarly, for the case with hexapole, the total outscattering from the upper Λ-doublet state to all other states except the lower Λ-doublet state is

$$\Delta N'_f = \sum_k \Delta N_k. \tag{11}$$

The scaling factor S can then be expressed as

TABLE III. Experimental results with their error and comparison to theory (Ref. 27) for scattering of OH with ''cold'' H_2. The initial states of OH are labeled by Ω, J, ϵ but the real initial population distribution is given in Table I, see also the text. The initial state distribution of H_2 is given in Table II. All values are given in $Å^2$.

Final state			Initial state: 3/2,3/2,f				Initial state: 3/2,3/2,e			
			Normal H_2		Para H_2		Normal H_2		Para H_2	
Ω	J	ϵ	Experimental	Theory	Experimental	Theory	Experimental	Theory	Experimental	Theory
3/2	3/2	f					8.17±0.42	7.297	4.61±0.29	6.239
	5/2	f	5.23±0.28	4.173	2.70±0.17	1.489	4.54±0.84	2.839	2.62±0.39	1.896
	7/2	f	1.14±0.06	0.994	0.73±0.05	0.515	0.00±0.31	0.389	0.00±0.25	0.216
	9/2	f	0.06±0.06	0.088	0.00±0.05	0.079	0.97±0.12	0.079	0.38±0.08	0.066
	3/2	e	8.17±0.42	7.297	4.61±0.29	6.239				
	5/2	e	4.31±0.22	5.007	5.07±0.31	5.551	3.88±0.69	5.058	1.74±0.51	2.031
	7/2	e	0.98±0.06	1.256	0.71±0.06	0.851	1.58±0.23	2.339	2.07±0.17	2.392
	9/2	e	0.14±0.05	0.413	0.33±0.05	0.410	0.95±0.12	0.338	0.74±0.09	0.256
1/2	1/2	f	1.18±0.08	0.889	0.44±0.04	0.489	2.21±0.28	2.226	2.30±0.16	2.937
	3/2	f	1.79±0.11	2.146	2.12±0.15	2.879	0.18±0.20	1.120	0.78±0.23	0.564
	5/2	f	0.51±0.05	0.697	0.32±0.04	0.441	0.82±0.12	0.947	1.25±0.11	1.137
	1/2	e	3.64±0.21	2.798	4.34±0.26	3.426	1.28±0.44	0.914	1.12±0.40	0.424
a	3/2	e	1.43±0.05	1.721	1.13±0.09	1.221	1.13±0.24	2.388	2.47±0.23	2.457

[a]The cross section at the $\frac{1}{2}$, $\frac{3}{2}$, e entry in fact represents the sum of the $\frac{3}{2}$ and $\frac{5}{2}$ states, see the text.

$$S=\frac{\Delta N_f}{\Delta N_f'}\frac{\Delta n_f'}{\Delta n_f}, \tag{12}$$

where $\Delta n_f'/\Delta n_f$ follows from Eqs. (6) (9), and (10)

$$\frac{\Delta n_f'}{\Delta n_f}=\frac{\Sigma_k \frac{\Delta n_k}{\Delta n_f}}{1+\frac{\Delta n_e'}{\Delta n_f'}}. \tag{13}$$

The only unknown quantity in this expression for S is the ratio $\Delta n_e'/\Delta n_f'$ To determine that ratio, we proceed as follows.

When comparing Eqs. (9) and (10) with Eqs. (4) and (5), it follows:

$$\frac{\Delta n_e'}{\Delta n_f'}=\frac{n_e\Sigma_k\sigma'_{e\to k}}{n_f\Sigma_k\sigma'_{f\to k}}=\frac{\Delta n_e+n_f\sigma'_{f\to e}-n_e\sigma'_{e\to f}}{\Delta n_f+n_e\sigma'_{e\to f}-n_f\sigma'_{f\to e}}. \tag{14}$$

The energy difference between the two Λ-doublet states is very small, so we can assume that $\sigma'_{e\to f}=\sigma'_{f\to e}=\sigma'_\Lambda$. When dividing the right hand side of Eq. (14) by $\Delta n_{f,\mathrm{out}}$, which is given by

$$\Delta n_{f,\mathrm{out}}=n_f\sigma'_{f\to e}+n_f\sum_i \sigma'_{f\to i} \tag{15}$$

it takes the form

$$\frac{\Delta n_e'}{\Delta n_f'}=\frac{\frac{\Delta n_e}{\Delta n_{f,\mathrm{out}}}+\frac{n_f\sigma'_\Lambda}{\Delta n_{f,\mathrm{out}}}\left(1-\frac{n_e}{n_f}\right)}{\frac{\Delta n_f}{\Delta n_{f,\mathrm{out}}}+\frac{n_f\sigma'_\Lambda}{\Delta n_{f,\mathrm{out}}}\left(\frac{n_e}{n_f}-1\right)}. \tag{16}$$

The quantity $\Delta n_{f,\mathrm{out}}\sigma'_\Lambda/n_f$ is in fact the relative Λ-doublet cross section as measured with hexapole, and it follows:

$$\frac{n_f\sigma'_\Lambda}{\Delta n_{f,\mathrm{out}}}=\sigma_\Lambda \tag{17}$$

by which Eq. (16) reduces to

$$\frac{\Delta n_e'}{\Delta n_f'}=\frac{\frac{\Delta n_e}{\Delta n_{f,\mathrm{out}}}+\sigma_\Lambda\left(1-\frac{n_e}{n_f}\right)}{\frac{\Delta n_f}{\Delta n_{f,\mathrm{out}}}+\sigma_\Lambda\left(\frac{n_e}{n_f}-1\right)}. \tag{18}$$

The quantity n_e/n_f is the ratio of the populations of the initial states, and is measured to be 0.68 ± 0.01. Making use of Eqs. (5), (15) and (17), it follows:

$$\frac{\Delta n_f}{\Delta n_{f,\mathrm{out}}}=\frac{\Delta n_{f,\mathrm{out}}-n_e\sigma'_\Lambda}{\Delta n_{f,\mathrm{out}}}=1-\sigma_\Lambda\frac{n_e}{n_f}, \tag{19}$$

$$\frac{\Delta n_e}{\Delta n_{f,\mathrm{out}}}=\frac{\Delta n_e}{\Delta n_f}\frac{\Delta n_f}{\Delta n_{f,\mathrm{out}}}=\frac{\Delta n_e}{\Delta n_f}\left(1-\sigma_\Lambda\frac{n_e}{n_f}\right). \tag{20}$$

The relation between $\Delta n_e'/\Delta n_f'$ and $\Delta n_e/\Delta n_f$ is then given by

$$\frac{\Delta n_e'}{\Delta n_f'}=\frac{\frac{\Delta n_e}{\Delta n_f}\left(1-\sigma_\Lambda\frac{n_e}{n_f}\right)+\sigma_\Lambda\left(1-\frac{n_e}{n_f}\right)}{1-\sigma_\Lambda}. \tag{21}$$

One can easily check that for $n_e=n_f$ Eq. (21) reduces to $\Delta n_e'/\Delta n_f'=\Delta n_e/\Delta n_f$.

With the determination of the scaling factor S, we can scale the data obtained with hexapole and subtract them from the data obtained without hexapole, according to Eq. (6):

$$\frac{\Delta n_{e\to k}}{\Delta n_f}=\frac{\Delta n_k}{\Delta n_f}-S\frac{\Delta N_k}{\Delta N_f}. \tag{22}$$

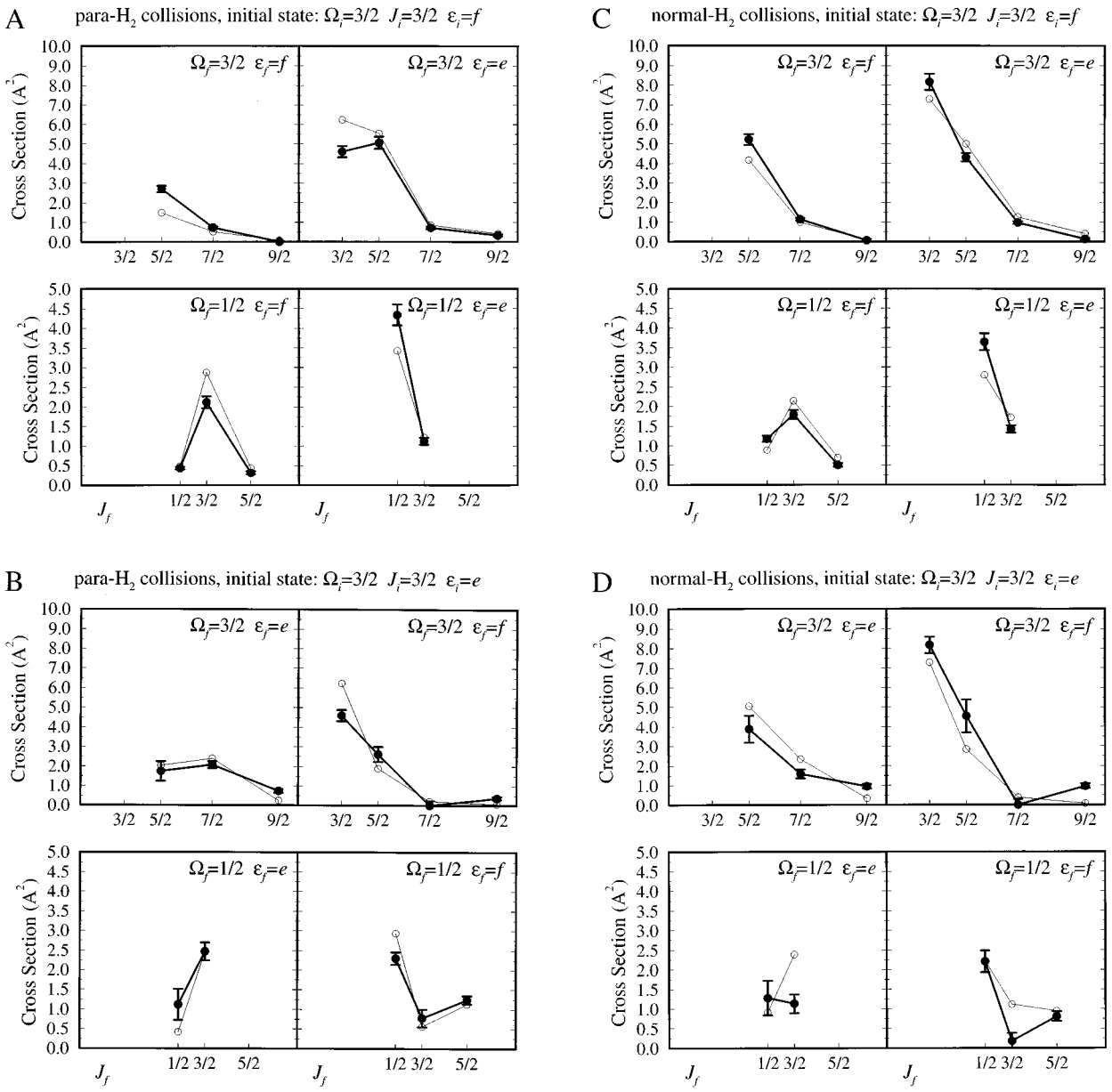

FIG. 4. Experimental (●) and theoretical (○) cross sections for rotational excitation of OH by ''cold'' H_2 at 595 cm^{-1}. The theoretical values are from Offer *et al.* (Ref. 27). All cross sections are in units of $Å^2$. Note that the J_f values are placed at positions given by the excitation energy.

Note that all quantities involved in the calculation of S are measured ones. Consequently, the cross sections for the transitions starting from the $\frac{3}{2},e$ state are determined in a purely experimental way.

In order to relate the cross sections for normal and para-H_2 the total cross sections in both cases were compared for the same H_2-density in the collision area.

III. RESULTS AND DISCUSSION

The measured cross sections obtained from the experiment with ''cold'' H_2 are presented in Table III. These values are also presented graphically in Fig. 4. In this figure the horizontal axis of the graphs is an energy scale on which the rotational quantum number of the final state is placed according to the difference in energy with the initial state. The vertical scale is in $Å^2$ which is based on the theoretical values by Offer *et al.*[27] The presented experimental values have been scaled to the theoretical ones by equalizing the sum of the experimental and theoretical values. The summation ranged over the whole set of data for ortho- and para-H_2. The ''warm'' set, which is presented in Table IV, and the ''cold'' set, however, were scaled separately. This scaling is made possible because, as described above, all measured cross sections are in the same units. We believe that this way of scaling is the least arbitrary and all information with regard to the relative sizes is conserved.

In the left two graphs of Fig. 4 the cross sections for para-H_2 collisions are shown and in the right part [Fig. 4(C)

TABLE IV. Experimental results with their error and comparison with theory (Ref. 27) for scattering of OH with ''warm'' H_2. The initial states of OH are labeled by Ω, J, ϵ but the real initial population distribution is given in Table I, see also the text. The initial state distribution of H_2 is given in Table II. All values are given in $Å^2$.

Final state			Initial state: 3/2,3/2,f				Initial state: 3/2,3/2,e			
			Normal H_2		Para H_2		Normal H_2		Para H_2	
Ω	J	ϵ	Experimental	Theory	Experimental	Theory	Experimental	Theory	Experimental	Theory
3/2	3/2	f					5.77±0.16	7.389	18.1±1.3	8.773
	5/2	f	4.82±0.19	3.884	3.26±0.43	1.923	2.52±0.79	3.041	1.51±0.92	2.015
	7/2	f	1.07±0.04	0.950	0.97±0.15	0.551	0.18±0.19	0.414	0.00±0.30	0.284
	9/2	f	0.12±0.03	0.125	0.12±0.08	0.108	0.14±0.11	0.090	0.16±0.10	0.090
	3/2	e	5.77±0.16	7.389	18.1±1.3	8.773				
	5/2	e	3.66±0.09	4.546	3.76±0.30	5.163	3.36±0.69	5.033	3.06±1.19	2.719
	7/2	e	1.40±0.04	1.259	0.92±0.11	1.038	1.46±0.26	2.271	1.33±0.39	2.223
	9/2	e	0.54±0.03	0.456	0.28±0.08	0.434	0.27±0.09	0.363	0.40±0.14	0.319
1/2	1/2	f	0.88±0.04	0.856	0.34±0.11	0.647	1.61±0.44	2.298	2.44±0.48	2.649
	3/2	f	1.26±0.04	1.941	0.70±0.14	2.626	1.29±0.19	1.212	2.40±0.55	0.764
	5/2	f	0.73±0.03	0.702	0.29±0.12	0.558	0.75±0.25	1.076	1.16±0.28	1.073
	1/2	e	3.55±0.09	2.498	2.02±0.20	3.042	0.47±0.29	0.943	1.88±0.69	0.592
a	3/2	e	1.44±0.04	1.766	0.95±0.11	1.497	1.72±0.31	2.415	2.08±0.53	2.456

[a]The cross section at the $\frac{1}{2}$, $\frac{3}{2}$, e entry in fact represents the sum of the $\frac{3}{2}$ and $\frac{5}{2}$ states, see the text.

and 4(D)] the cross sections for normal-H_2 collisions. The graphs on the upper part [Fig. 4(A) and 4(C)] show the cross sections for transitions starting from the $\frac{3}{2},f$ state and the lowest two graphs show the cross sections for transitions starting from the $\frac{3}{2},e$ state. Each graph is divided into four quadrants where the upper two show the data for multiplet conserving transitions and the lower two show the data for multiplet changing transitions. In the left two quadrants the cross sections for symmetry conserving transitions are presented and on the right hand side the cross sections for symmetry changing transitions. The data point at $J=\frac{3}{2}$ in the upper two quadrants represents the Λ-doublet cross section.

From Fig. 4 it is seen that the cross sections for multiplet changing transitions are on the average a factor of 2 smaller than those for multiplet conserving transitions. For multiplet *conserving* transitions the cross section decreases with the difference in energy, which would be expected if an energy gap law[39] is valid. However in the case of the $\frac{3}{2}$, e state as the initial state some deviations are observed, as for the transition to the $\frac{9}{2}$, f state which has a larger cross section than the transition to the $\frac{7}{2}$, f state. There is no clear propensity with respect to parity or symmetry.

For multiplet *changing* transitions a different behavior is shown. The cross section for the transition to $J=\frac{3}{2}$ is large in the case of equal symmetry of initial and final state but small when symmetry changes. This indicates that symmetry is preferentially conserved in case of $\Delta J=0$, whereas the symmetry is changed in the case of $\Delta J=\pm 1$. Whether this holds more general for ΔJ is even or odd, respectively, will be clear when more data points are available.

When comparing $e\rightarrow f$ scattering with $f\rightarrow e$ scattering at the same rotational transition, it is seen that roughly the same collisional behavior is observed, but quantitative differences are present. The reason behind the differences of the two lies in the mixed Hund's case (a) and (b) character of OH. Only for pure type (a) molecules one expects $e\rightarrow f$ scattering to be the same as $f\rightarrow e$ scattering.[40] It is these differences which are responsible for the fact that collisions might be the mechanism behind a population inversion of OH in the interstellar space.

Much to our surprise para- and normal-H_2 scattering show roughly the same behavior. However, large differences are observed for the Λ-doublet transition and the $\frac{3}{2}$, $\frac{3}{2}$, $e\rightarrow\frac{1}{2}$, $\frac{3}{2}$, e transition, and, to a lesser extent, the $\frac{3}{2}$, $\frac{3}{2}$, $f\rightarrow\frac{3}{2}$, $\frac{5}{2}$, f and $\frac{3}{2}$, $\frac{3}{2}$, $e\rightarrow\frac{3}{2}$, $\frac{5}{2}$, e transitions. The Λ-doublet cross section for para-H_2 scattering increases strongly when heating the para-H_2, as can be seen from Fig. 5 where the results for scattering of the $\frac{3}{2}$, e state by ''warm'' para-H_2 are presented. This behavior can therefore be attributed to the presence of higher rotational states ($J=2,3$) in the para-H_2 beam and the conclusion can be drawn that for pure para-H_2 ($J=0$) scattering the Λ-doublet cross section is very small. When this is taken into account, para-H_2 ($J=0$) scattering and He scattering, which is shown in Fig. 6 show a very similar behavior. This has long been assumed from a theoretical point of view,[29] based on the fact that the quadrupole moment of $H_2(J=0)$ does not play a role in inelastic scattering and consequently this molecule behaves like a spherical symmetric particle. This has now been shown experimentally.

We have compared our experimental data to the results of quantum calculations by Offer *et al.*[27] which are based on their *ab-initio* OH–H_2 potential.[26] In addition to their published results, some new calculations have been performed at our translational energies and for H_2 ($J=3$) scattering.[41] The theoretical values to which we compare, are constructed by summing the state-to-state values according to the measured initial state distributions of both the OH and the H_2 beams.

The overall correspondence between experiment and theory is surprisingly good, as can be seen from Figs. 4 and 5. Most trends and relative sizes are predicted accurately. The agreement is better for ''cold'' H_2 than for ''warm'' H_2. Probably the $J=2$ calculations are less accurate than the

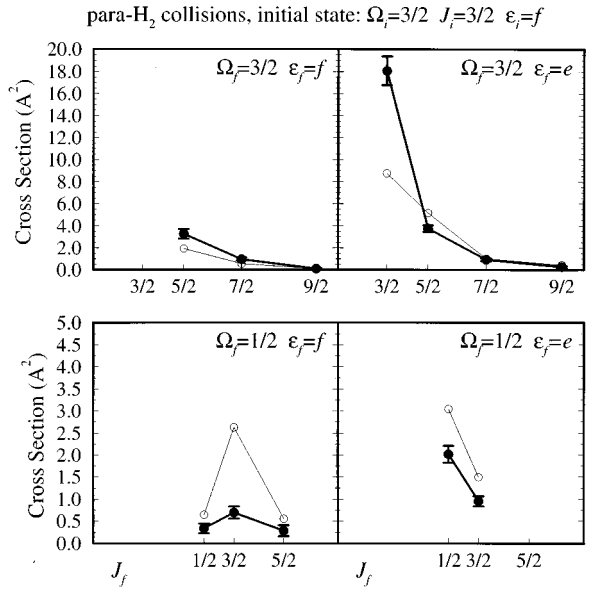

FIG. 5. Experimental and theoretical cross sections for OH($\frac{3}{2},f$)+ ''warm'' para-H_2 scattering at 595 cm^{-1}. The theoretical values are from Offer *et al.* (Ref. 27). Note the change of the vertical scale in the upper part of the figure with respect to Fig. 4.

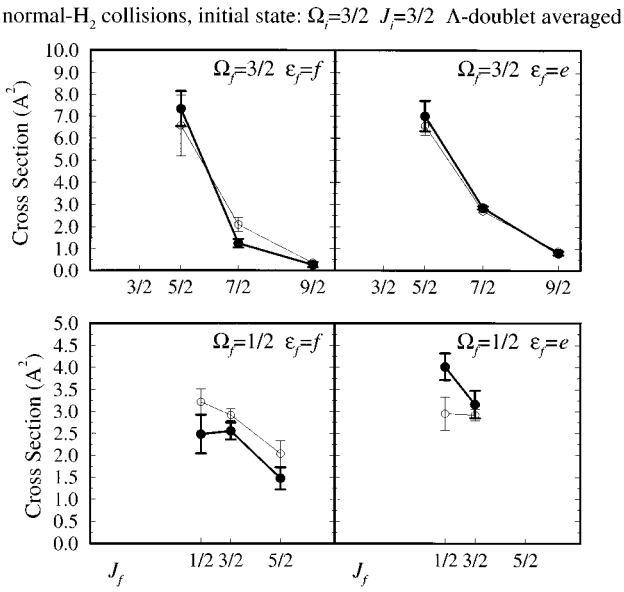

FIG. 7. Measured Λ-doublet averaged cross sections for OH scattering by H_2. The filled circles (●) represent the present data for ''warm'' H_2. The open circles (○) are taken from Andresen *et al.* (Ref. 20).

ones for $J=0$ and $J=1$. A reason for this could be the fact that for $J=2$ the total (i.e., translational and internal) energy of the system is so high that a larger number of basis functions should be taken into account. Individual points which deviate are the $\frac{3}{2}$, $\frac{3}{2}$, $e\rightarrow\frac{1}{2}$, $\frac{3}{2}$, e and f transitions for normal-H_2, whereas the same cross sections show a good correspondence in the case of para-H_2. For the $\frac{3}{2}$, $\frac{3}{2}$, $f\rightarrow\frac{3}{2}$, $\frac{5}{2}$, f transition it is the other way around.

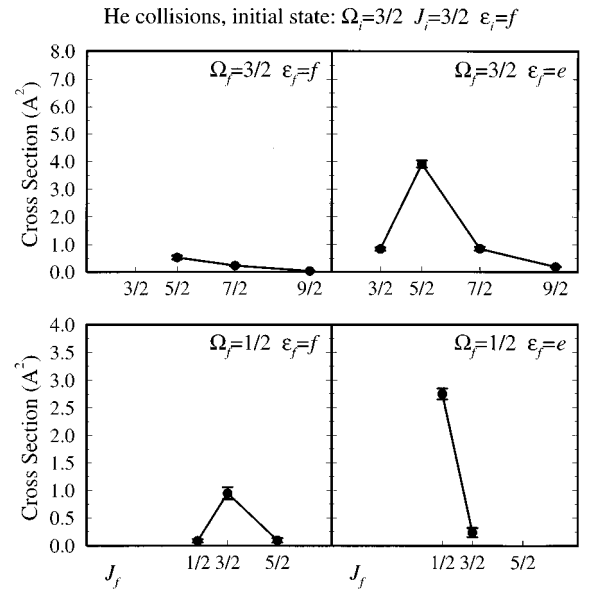

FIG. 6. Measured cross sections for OH($\frac{3}{2},e$) + He scattering at 394 cm^{-1}. These are values from a previous paper (Ref. 30).

Recently also values by Miller *et al.*[11] have been published, based on the *ab-initio* potential of Kliesch and Werner.[11] Unfortunately, they have provided only data for scattering with H_2 in $J=0,1$ where data for H_2 in $J=2,3$ are needed to compare our experimental data with their calculated values. A comparison between their results, the corresponding ones of Offer *et al.*, and our values, yielded a better agreement between experiment and theory for the values of Offer *et al.* However, because of the lack of H_2 ($J=2,3$) data in the work of Miller and Clary, no hard conclusion on this can be drawn. Also one has to remind that the potential developed by Kliesch and Werner was designed primarily for a description of the van der Waals complex, and to a lesser extent for collisional dynamics, where a much larger range of the potential contributes to the scattering process. The out of plane OH–H_2 configurations which Offer *et al.* took into account in their *ab-initio* potential might yield a better description of the collision process.

In Fig. 7 a comparison is made with the data of Andresen *et al.*[20] For this purpose we have summed our cross sections for both initial states, assuming their initial population is an equal mixture of $\frac{3}{2}$, e and $\frac{3}{2}$, f as was the case in the experiment of Andresen *et al.*, where, different from the present experiment, the OH molecules were produced by photolysis. For the secondary beam we have considered ''warm'' normal H_2, as, most probably, was the situation in their experimental setup. The different measurements agree very well. Some deviations show up for the cross sections for multiplet changing transitions. Whereas the present averaged cross section for transitions to the $\frac{1}{2}$, $\frac{1}{2}$, f state is smaller than the result of Andresen *et al.*, the opposite situation is present for the transition to the $\frac{1}{2}$, $\frac{1}{2}$, e state. This may affect the astrophysical implications, as is clarified when considering the ratios of the cross sections for transitions to the lower and

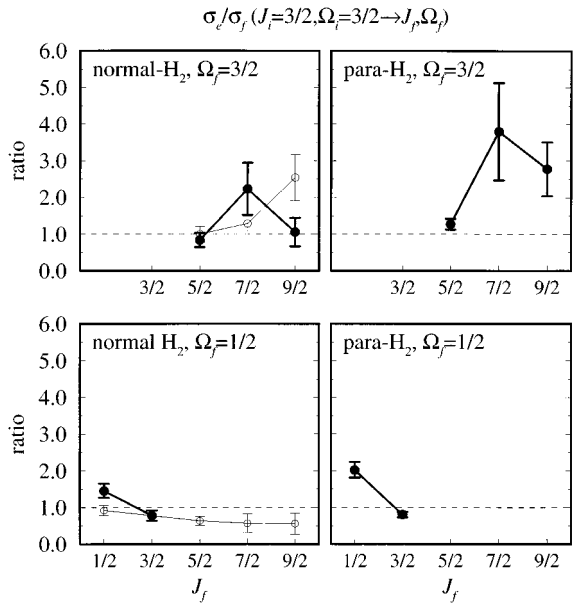

FIG. 8. Ratio of experimental cross sections for transitions from the lowest rotational state to the lower and upper Λ-doublet states. The population in the initial state is equal for each Λ-doublet substate. The filled circles (●) represent our ''warm'' data. The open circles (○) are taken from Andresen *et al.* (Ref. 16).

upper Λ-doublet states. These ratios are presented in Fig. 8 (for ''warm'' H_2) and are compared to the results of Andresen *et al.*[20] Globally it can be concluded that transitions to the lowest Λ-doublet state are favored. This could imply that collisional excitation is *not* the main mechanism behind the interstellar population inversion of OH. This was already concluded by Andresen *et al.* for the $\Omega=\frac{3}{2}$ states, but not for the $\Omega=\frac{1}{2}$ states where they found a preference for the upper Λ-doublet states. Also for para-H_2 the present Λ-doublet averaged results show a propensity for the lower Λ-doublet states, as can be seen from Fig. 8.

The astrophysical implications are difficult to predict. The best way to model OH masers is by incorporating collisional (de-)excitation of OH by H_2 in a large scale model which also includes the various effects of OH creation and ir radiation, like Cesaroni and Walmsley did.[3] The observed large difference between the Λ-doublet cross sections for scattering by ortho- and para-H_2 will probably affect the outcome of new calculations, because this difference has not been predicted before by the theoretical results used in previous calculations.

IV. CONCLUSION

In this experiment cross sections have been determined for rotational excitation of OH by normal- and para-H_2 in a crossed beam experiment. A full characterization of the initial states of both the OH and H_2 beams gives a good insight in the state-to-state cross sections and allows a detailed comparison with theory. Cross sections were obtained for OH in both $J=\frac{3}{2}$ Λ-doublet states by combining results obtained with electrostatic hexapole state selection with results obtained without state selection.

The present measurements show a very similar result for para-H_2 ($J=0$) scattering and Helium scattering, as has been assumed previously, based on theoretical arguments. In both cases a relatively small cross section is measured for the Λ-doublet transition. This is in sharp contrast to scattering by H_2 in excited rotational states, where the cross section for the Λ-doublet transition is by far the largest. Possibly this is caused by the quadrupole moment of H_2 which does not contribute to the scattering process for $J=0$. The effect of a deviation from the $1\div3$ equilibrium distribution of para- and ortho-H_2 on the outcome of the collision process is restricted to mainly this Λ-doublet transition. This may have some implications with regard to the role of collisional pumping in the model of interstellar OH masers.

When no other physical processes than collisions are considered in interstellar OH sources, these results lead to the conclusion that collisions do not tend to create a population inversion for OH at our collisional energy. In interstellar space however, different collisional energies and ''initial'' populations are present and this will affect this conclusion. Conclusions should await the results of modeling studies in which also radiative pumping is taken into account.

The theoretical values of Offer and Van Hemert[27] show a surprisingly good agreement with the present experimental values. Deviations can be ascribed partly to inaccuracies in the H_2 ($J=2$) calculations. The validation of the theoretical cross sections by the present measurements gives a strong stimulus to extrapolate the calculations to interstellar relevant collision energies.

ACKNOWLEDGMENTS

We wish to express our gratitude to Dr. M. van Hemert for calculating the experiment specific cross sections and to Mr. E. van Leeuwen for his expert technical assistance.

[1] P. Andresen, Astron. Astrophys. **154**, 42 (1986).
[2] N. D. Kylafis and C. A. Norman, Astrophys. J. **350**, 209 (1990).
[3] R. Cesaroni and C. M. Walmsley, Astron. Astrophys. **241**, 537 (1991).
[4] M. Elitzur, Annu. Rev. Astron. Astrophys. **30**, 75 (1992).
[5] H. Szichman and M. Bär, J. Chem. Phys. **101**, 2081 (1994), and the references therein.
[6] N. Balakrishnan and G. D. Billing, J. Chem. Phys. **101**, 2785 (1994).
[7] D. H. Zhang and J. Z. H. Zhang, J. Chem. Phys. **101**, 2785 (1994). D. H. Zhang, J. Z. H. Zhang, Y. Zhang, D. Wang, and Q. Zhang, *ibid.* **102**, 7400 (1995).
[8] T. N. Truong, J. Chem. Phys. **102**, 5335 (1995).
[9] R. A. Loomis and M. I. Lester, J. Chem. Phys. **103**, 4317 (1995).
[10] S. M. Miller and D. C. Clary, J. Chem. Phys. **98**, 1843 (1993).
[11] S. M. Miller, D. C. Clary, A. Kliesch, and H.-J. Werner, Mol. Phys. **83**, 405 (1994).
[12] R. Hernandez and D. C. Clary, Chem. Phys. Lett. **244**, 421 (1995).
[13] W. D. Gwinn, B. E. Turner, W. M. Gars, and G. L. Blackman, Astrophys. J. **179**, 789 (1973).
[14] M. Bertojo, A. C. Cheung, and C. H. Townes, Astrophys. J. **208**, 914 (1976).
[15] M. H. Alexander and P. J. Dagdigian, J. Chem. Phys. **80**, 4325 (1984).
[16] R. Schinke and P. Andresen, J. Chem. Phys. **81**, 5644 (1984).
[17] G. Diehler and W.H. Kegel, Astron. Astrophys. **214**, 339 (1989).
[18] M. D. Gray, D. Field, and R.C. Doel, Astron. Astrophys. **262**, 555 (1992).

[19] A. R. Offer and E. F. van Dishoeck, Mon. Not. R. Astr. Soc. **257**, 377 (1992).
[20] P. Andresen, D. Haüsler, and H. W. Lülf, J. Chem. Phys. **81**, 571 (1984).
[21] P. Andresen, N. Aristov, V. Beushausen, D. Häusler, and H. W. Lülf, J. Chem. Phys. **95**, 5763 (1989).
[22] G. C. Corey and M. H. Alexander, J. Chem. Phys. **88**, 11 (1988).
[23] D.P. Dewangan, D. R. Flower, and G. Danby, J. Phys. B **19**, L747 (1986).
[24] A. Offer and D. R. Flower, J. Phys. B **23**, L391 (1990).
[25] E. Koschanski and D. R. Flower, Chem. Phys. **57**, 217 (1981).
[26] A. R. Offer and M. C. van Hemert, J. Chem. Phys. **99**, 3836 (1993).
[27] A. R. Offer, M. C. van Hemert, and E. F. van Dishoeck, J. Chem. Phys. **100**, 362 (1994).
[28] G. Pineau des Forêts, D. R. Flower, and R. McCaroll, Mon. Not. R. Astr. Soc. **248**, 173 (1991).
[29] T. Oka, Adv. At. Mol. Phys. **9**, 127 (1973).
[30] K. Schreel, J. Schleipen, A. Eppink, and J. J. ter Meulen, J. Chem. Phys. **99**, 8713 (1993).
[31] J. Schleipen and J. J. ter Meulen, Chem. Phys. **156**, 479 (1991).
[32] G. H. Dieke and H. M. Crosswhite, J. Quant. Spectrosc. Radiat. Transfer **2**, 97 (1962).
[33] I. F. Silvera, Rev. Mod. Phys. **52**, 393 (1980).
[34] W. C. Wiley and I. H. McLaren, Rev. Sci. Instrum. **26**, 1150 (1955).
[35] E. W. Rothe, G. S. Ondrey, and P. Andresen, Opt. Comm. **58**, 113 (1986).
[36] D. J. Kligler and C. K. Rhodes, Phys. Rev. Lett. **40**, 309 (1978).
[37] L. M. Hitchcock, G.-S. Kim, E. W. Rothe, and G. P. Reck, Appl. Phys. B **52**, 27 (1991).
[38] S. T. Pratt, P. M. Dehmer, and J. L. Dehmer, Chem. Phys. Lett. **105**, 28 (1984).
[39] R. D. Levine and R. B. Bernstein, *Molecular Reaction Dynamics and Chemical Reactivity* (Oxford University Press, Oxford, 1987).
[40] P. J. Dagdigian, M. H. Alexander, and K. Liu, J. Chem. Phys. **91**, 839 (1989).
[41] M. van Hemert (private communication).